

Entanglement Entropy Near Cosmological Singularities

Netta Engelhardt and Gary T. Horowitz

Department of Physics, UCSB, Santa Barbara, CA 93106, USA

engeln@physics.ucsb.edu, gary@physics.ucsb.edu

Abstract

We investigate the behavior of the entanglement entropy of a confining gauge theory near cosmological singularities using gauge/gravity duality. As expected, the coefficients of the UV divergent terms are given by simple geometric properties of the entangling surface in the time-dependent background. The finite (universal) part of the entanglement entropy either grows without bound or remains bounded depending on the nature of the singularity and entangling region. We also discuss a confinement/deconfinement phase transition as signaled by the entanglement entropy.

Contents

1	Introduction	2
2	Cosmological backgrounds and extremal surfaces	3
2.1	Finding the Extremal Surfaces	5
3	Results	8
3.1	Confinement/deconfinement transition	8
3.2	Entanglement entropy	9

1 Introduction

There has been considerable interest recently in the entanglement entropy of quantum field theories. Entanglement entropy is a measure of long range correlations in the system which has proven useful in a variety of applications including identifying exotic ground states [1, 2] and signaling phase transitions. In particular, it has been shown [3, 4, 5] that a confinement/deconfinement phase transition, which is usually studied at finite temperature, can be detected in the zero temperature ground state by studying the entanglement entropy for regions of various sizes.

We explore another potential application of the entanglement entropy: probing cosmological singularities. Understanding past spacelike (“big bang”) singularities is a long-standing goal of quantum gravity. While much progress has been made in understanding static timelike singularities in string theory, spacelike singularities remain mysterious. There have been various attempts to resolve spacelike singularities using gauge/gravity duality (see, e.g., [6, 7, 8, 9]) but we will be less ambitious here. Rather than attempt to resolve cosmological singularities, we will endeavor to understand one of their effects on a quantum field theory. We compute the entanglement entropy for a confining gauge theory in a class of fixed (classical) cosmological backgrounds. As we will discuss, the choice of a confining gauge theory has technical advantages for the calculation, but it is also of particular physical interest since it models an early-universe quark-gluon plasma. The quark-gluon plasma is expected to feature a mass gap and a confinement/deconfinement phase transition at around 150 MeV [10].

Given a state of a quantum field theory and a region of space, \mathcal{R} , the entanglement entropy measures the quantum entanglement of the part of the state in \mathcal{R} with the rest of the state in $\bar{\mathcal{R}}$, the complement of \mathcal{R} . It is defined in terms of the von Neumann entropy of the reduced density matrix on \mathcal{R} :

$$S_{EE} = -\text{Tr}(\rho_{\mathcal{R}} \ln \rho_{\mathcal{R}}) \tag{1.1}$$

where $\rho_{\mathcal{R}} = \text{tr}_{\bar{\mathcal{R}}}\rho$. While S_{EE} is a divergent quantity due to the short-wavelength modes across $\partial\mathcal{R}$ and must be regulated, it is generally possible to extract its universal (UV cutoff-independent) component.

Calculating S_{EE} in strongly coupled theories using the field theory formalism, however, is notoriously difficult. We will therefore calculate S_{EE} using the more tractable holographic approach

instead. The original Ryu-Takayanagi formulation [11] of holographic entanglement entropy states that the entanglement entropy of a region \mathcal{R} in a field theory dual to some static asymptotically locally AdS $_{d+1}$ bulk spacetime is proportional to the area of a minimal surface homologous to the entangling region on the boundary:

$$S_{EE} = \frac{\text{Area}(\gamma_{\mathcal{R}})}{4G_N^{(d+1)}} \quad (1.2)$$

where $\gamma_{\mathcal{R}}$ is the minimal area surface in the bulk and $G_N^{(d+1)}$ is the $(d+1)$ -dimensional Newton's constant¹. In this proposal, the classical bulk spacetime is static, so there is a canonical time slicing; the region \mathcal{R} and the corresponding minimal surface $\gamma_{\mathcal{R}}$ both lie on the same constant time slice. The more general, covariant Hubeny-Rangamani-Takayanagi prescription calls for the minimal surface $\gamma_{\mathcal{R}}$ to be replaced by an extremal surface; if several exist, the one with minimal area is chosen [12]. Since we work in cosmological backgrounds, we will employ the covariant proposal here.

There have been earlier studies of entanglement entropy in time-dependent backgrounds, e.g., [13, 14, 15, 16, 17, 18, 19, 20, 21, 22], but to our knowledge, none have explored the behavior near singularities.²

The area of any bulk surface which extends all the way to the boundary at infinity diverges, and this divergence obeys [24]:

$$\text{Area}(\gamma_R) = \frac{c_{d-2}}{\epsilon^{d-2}} + \frac{c_{d-4}}{\epsilon^{d-4}} + \dots + \begin{cases} c_0 \log\left(\frac{L}{\epsilon}\right) + \dots & d \text{ is even} \\ c_0 + \dots & d \text{ is odd} \end{cases} \quad (1.3)$$

where L is the length characterizing \mathcal{R} , ϵ is a UV cutoff, and the dots in the brackets represent terms that vanish as we take ϵ to zero. If a boundary-covariant cutoff is used, the coefficients c_i of the divergent terms are integrals of geometric quantities. In particular, the leading coefficient is proportional to the area of the boundary of the entangling region, $\partial\mathcal{R}$. We will work with $d=5$ and determine the c_1 coefficient as well as the UV cutoff-independent c_0 as functions of time in a class of cosmological backgrounds.

We treat the bulk geometry classically, but expect stringy and quantum corrections to be important very close to the singularity. We will stay away from this poorly understood region and only consider the entanglement entropy for times where the extremal surface stays in a region of the bulk where classical general relativity is valid.

2 Cosmological backgrounds and extremal surfaces

We wish to calculate the entanglement entropy for a field theory in a Kasner $_{3+1} \times S^1$ background:

$$ds_{\text{bdy}}^2 = -dt^2 + t^{2p_1} dx^2 + t^{2p_2} dy_1^2 + t^{2p_3} dy_2^2 + d\theta^2 \quad (2.1)$$

¹Note that this proposal admits quantum and stringy corrections when the bulk spacetime is not taken to obey classical general relativity.

²The interesting recent paper [23] considered the contribution to entanglement from the region inside black holes, but the extremal surfaces were bounded away from the singularity in the bulk.

where three of the spatial directions are periodically identified:

$$\begin{aligned}\theta &\sim \theta + L_0 \\ y_1 &\sim y_1 + L_1 \\ y_2 &\sim y_2 + L_2\end{aligned}$$

and the exponents p_i obey the Kasner conditions:

$$\sum_i p_i = 1 = \sum_i p_i^2 \quad (2.2)$$

These last conditions ensure that the metric is Ricci flat. This spacetime describes a homogeneous but anisotropic cosmology and generically has a curvature singularity at $t = 0$. The constant t surfaces are flat, but space expands at different rates in different directions. Since there are two conditions on the three exponents p_i , there is a one parameter family of solutions labeled, e.g., by p_1 which can range from $-1/3$ to 1. Generically at least one p_i is negative and the rest are positive, so one direction contracts while others expand. The only exception is when two of the exponents vanish and one recovers the Milne solution, which is locally flat. This is the only case in which $t = 0$ is not a curvature singularity.

We choose our entangling region, denoted $\mathcal{R}(t_b, x_0)$, to be a strip which is extended in all spatial directions except one, on a fixed time slice $t = t_b$:

$$\mathcal{R}(t_b, x_0) = \begin{cases} x \in [-x_0, x_0] \\ \theta \in [0, L_0] \\ y_1 \in [0, L_1] \\ y_2 \in [0, L_2] \\ t = t_b \end{cases} \quad (2.3)$$

It is the goal of this paper to calculate the entanglement entropy of $\mathcal{R}(t_b, x_0)$ holographically as a function of t_b . To do so, we must first find a bulk dual to the $\text{Kasner}_{3+1} \times S^1$ background.

We start with the AdS_6 soliton metric [25, 26], obtained by analytically continuing the timelike direction and one spatial direction from the planar AdS black hole:

$$ds_{\text{soliton}}^2 = \frac{1}{z^2} \left[(1 - z^5) d\theta^2 + \eta_{\mu\nu} dx^\mu dx^\nu + \frac{dz^2}{1 - z^5} \right] \quad (2.4)$$

where the AdS radius and black hole horizon radius have both been set to one. The θ circle smoothly caps off at $z = 1$, provided we set $L_0 = \frac{4\pi}{5}$, i.e., we periodically identify $\theta \sim \frac{4\pi}{5} + \theta$. This solution describes a confining vacuum in the dual field theory which lives on $\mathbb{R}^{3,1} \times S^1$. One can change the boundary metric by using the fact that replacing $\eta_{\mu\nu}$ in (2.4) with any (3,1)-dimensional, Ricci-flat solution of Einstein's equations still results in a bulk metric which is an exact solution of Einstein's equations with a negative cosmological constant. Replacing $\eta_{\mu\nu}$ with Kasner yields the (5 + 1)-dimensional Kasner-AdS soliton:

$$ds_{\text{KAS}}^2 = \frac{1}{z^2} \left(\frac{dz^2}{1 - z^5} - dt^2 + t^{2p_1} dx^2 + t^{2p_2} dy_1^2 + t^{2p_3} dy_2^2 + (1 - z^5) d\theta^2 \right) \quad (2.5)$$

This solution has a spacelike singularity at $t = 0$ which extends across the entire spacetime.

We could have started with AdS in Poincaré coordinates, and replaced the Minkowski metric on each constant radial surface with Kasner. The result is again a solution of Einstein's equation with negative cosmological constant. This would be dual to a nonconfining gauge theory on the Kasner spacetime. However, in addition to the singularity at $t = 0$, this solution has singularities on the Poincaré horizon which appear to be unphysical. These unphysical singularities are removed in (2.5) since the radial direction is capped off and there is no Poincaré horizon. Another advantage of starting with the AdS soliton is that since it is a confining geometry, it can be used to probe the confinement/deconfinement phase transition.

The proposal in [12] dictates that entanglement entropy be calculated from the area of an extremal surface homologous to the entangling region. We use the symmetries of the surface and the bulk metric to parametrize the surface in terms of the distinguished boundary coordinate x :

$$X^\mu = (t, x, \theta, y_1, y_2, z) = (T(x), x, \theta, y_1, y_2, Z(x)) \quad (2.6)$$

The induced metric on the surface $\gamma_{ab} = \partial_a X^\mu \partial_b X^\nu g_{\mu\nu}$, where $g_{\mu\nu}$ is the bulk metric, gives rise to the area functional for (2.6):

$$A = \frac{4\pi L_1 L_2}{5} \int_0^{x_0} dx \frac{T(x)^{1-p_1}}{Z(x)^4} [(1 - Z(x)^5) (T(x)^{2p_1} - T'(x)^2) + Z'(x)^2]^{\frac{1}{2}} \quad (2.7)$$

The set $\{T(x), Z(x)\}$ which solves the equations of motion generated by (2.7) and obeys the following boundary conditions

$$\begin{aligned} Z(x = \pm x_0) &= 0 \\ T(x = \pm x_0) &= t_b \end{aligned} \quad (2.8)$$

describes the extremal surface that enters into (1.2).

We pause here to note that the integral in (2.7) diverges and must be regulated. It is conventional to impose a UV cutoff some small distance away from the boundary $z = \epsilon$, which is the same UV cutoff that appears in the expansion (1.3). The integral in (2.7), however, is over the variable x , so we define the UV cutoff to be the value $z = \epsilon$ such that $Z(x_0 - \delta) = \epsilon$. We then integrate up to $x = x_0 - \delta$ instead of up to x_0 .

2.1 Finding the Extremal Surfaces

The equations of motion generated by (2.7) are a set of two coupled second order ordinary differential equations for which an analytical solution is not known. The general solution depends on four parameters, but the local boundary conditions (2.8) reduce this to two. We will generate a 2-parameter family of approximate solutions to the equations of motion by truncating a set of series expansions, and then use numerics to determine those two parameters for different values of the power p_1 and the time slice of the entangling region t_b . We now describe this procedure in more detail. Since it is valid in arbitrary dimension, in this subsection we work in general d .

We first solve the equations of motion for the surface via power series expansions. Integer power series, however, cannot represent nonanalytic functions. Since extremal surfaces in pure AdS are nonanalytic at the boundary and the Kasner-AdS soliton is asymptotically locally AdS, we expect extremal surfaces in (2.5) to have the same nonanalytic asymptotic behavior. We therefore investigate the asymptotic behavior of $T(x)$ and $Z(x)$ to find the corresponding fractional power series.

To probe the asymptotic behavior of $T(x)$, consider the AdS $_{d+1}$ soliton metric (2.4) in Milne coordinates:

$$ds^2 = \frac{1}{z^2} \left((1 - z^d) d\theta^2 + \frac{dz^2}{1 - z^d} - dt^2 + t^2 dx^2 + dy_1^2 + dy_2^2 \right) \quad (2.9)$$

Implementing a simple coordinate redefinition, we obtain the manifestly static soliton:

$$\begin{aligned} \chi &= t \sinh x \\ \tau &= t \cosh x \end{aligned} \quad (2.10)$$

$$ds^2 = \frac{1}{z^2} \left((1 - z^d) d\theta^2 + \frac{dz^2}{1 - z^d} - d\tau^2 + d\chi^2 + dy_1^2 + dy_2^2 \right) \quad (2.11)$$

The boundary condition $T(x = \pm x_0) = t_b$ in the Milne soliton corresponds to a boundary condition $\tau(x = \pm x_0) = t_b \cosh x_0$ in the soliton. The soliton, however, is static, so the entire extremal surface rests on the time slice $\tau = t_b \cosh x_0$. Using (2.10), we obtain an equation for $T(x)$:

$$T_{\text{Milne}}(x) = t_b \cosh x_0 \operatorname{sech} x \quad (2.12)$$

$T(x)$ is therefore analytic in the Milne soliton. We expect that, for the Kasner-AdS soliton, $T(x)$ is analytic as well, and can be expanded:

$$T(x) = \sum_{i=0}^{\infty} T_i (x_0^2 - x^2)^i \quad (2.13)$$

where the x^2 term results from $T(x) = T(-x)$ by reflection symmetry of the entangling region.

The exact solution for $x(Z)$ is known in pure AdS [27]:

$$\pm x(Z) = \frac{Z^d}{dz_*^{d-1}} {}_2F_1 \left[\frac{1}{2}, \frac{d}{2(d-1)}, \frac{3d-2}{2(d-1)}, \frac{Z^{2(d-1)}}{z_*^{2(d-1)}} \right] - z_* \frac{\sqrt{\pi} \Gamma \left[\frac{3d-2}{2(d-1)} \right]}{d \Gamma \left[\frac{2d-1}{2(d-1)} \right]} \quad (2.14)$$

where

$$z_* = 2x_0 \frac{(d-1) \Gamma \left[\frac{2d-1}{2(d-1)} \right]}{\sqrt{\pi} \Gamma \left[\frac{d}{2(d-1)} \right]} \quad (2.15)$$

is the turning point of the surface and ${}_2F_1$ is a hypergeometric function. We expand the solution in a Taylor series about the point x_0 and then take the inverse series to obtain an expansion for $Z(x)$:

$$Z(x) = (x_0^2 - x^2)^{1/d} \sum_{i=0}^{\infty} Z_i (x_0^2 - x^2)^{\frac{i}{d}} \quad (2.16)$$

where the Z_i are constants. We expect a similar asymptotic behavior in the Kasner-AdS soliton. Indeed, substituting the expansions (2.13) and (2.16) into the equations for the extremal surface results in a two parameter family of solutions. The remaining two parameters are fixed by requiring regularity at the origin. This is difficult to impose starting with local power series expansions about $\pm x_0$, so we turn to numerical methods.

One can make the expansion for $Z(x)$ analytic by introducing a new coordinate \tilde{x} defined by $(x_0^2 - x^2)^{\frac{1}{d}} = (1 - \tilde{x}^2)$. The equations of motion remain analytic in \tilde{x} and we have

$$Z(\tilde{x}) = (1 - \tilde{x}^2) \sum_{i=0}^{\infty} \tilde{Z}_i (1 - \tilde{x}^2)^i = (1 - \tilde{x}^2) P(\tilde{x}) \quad (2.17)$$

The factor of $(1 - \tilde{x}^2)$ on the right is convenient since then $P(\pm 1)$ is nonzero. Since $P(\tilde{x})$ is analytic everywhere, we can solve for it and $T(\tilde{x})$ numerically using pseudospectral methods. For a single connected extremal surface, this is most conveniently done by taking advantage of the reflection symmetry about $x = 0$ and just solving the equations for x in $[0, x_0]$ with boundary conditions $T'(0) = 0, Z'(0) = 0, T(x_0) = t_b$ and $Z(x_0) = 0$. We have checked our numerics by comparing the numerical solutions with known exact solutions in special cases. Our numerical solutions for $Z(x)$ in pure AdS and $T(x)$ in the Milne soliton agree with the known solutions to order 10^{-14} . We solve the equations of motion for a range of the parameters p_1 and t_b . By comparing the power series solutions with the numerical results, we fix the two free parameters in those solutions.

The reason that we choose to work with analytical power series rather than the numerical solutions is that numerical integration of the surfaces is difficult to perform accurately due to the steepness of the surfaces at boundary. In particular, extracting the dependence of the area on the cutoff is delicate to do numerically, and much more accurate results can be obtained from the power series as follows. We compute the area by substituting the (truncated) series expansions for $T(x)$ and $Z(x)$ into (2.7), expand the functional in polynomials, and integrate analytically from $x = 0$ to $x = x_{UV}$, where x_{UV} is a symbolic parameter without an assigned numerical value. The analytical form of the integral $A(x)$ is a power series in x_{UV} :

$$A(x_{UV}) = \sum_i A_i (x_0 - x_{UV})^{\frac{i}{d}} \quad (2.18)$$

where the A_i are numerical coefficients. In order to determine the area's UV cutoff-dependent and independent behavior, the area $A(x_{UV})$ must be expressed as a function of Z . To accomplish this, we obtain a series expansion for $x(Z)$ by inverting the series $Z(x)$ via a variable change $(x_0^2 - x^2)^{1/d} = x_0^2 - y^2$, so that we have, as before, an analytic series expansion for Z :

$$Z(y) = \sum_i \mathcal{Z}_i (x_0^2 - y^2)^i \quad (2.19)$$

Since this series is analytic, we can easily obtain the inverse series $y(Z)$ and the area $A(x(y(Z))) = A(Z)$ as a function of the bulk coordinate Z . A Taylor expansion of $A(Z)$ around $Z = 0$ yields the expected behavior (1.3). This allows us to immediately read off the leading divergent, subdivergent,

and constant pieces for a choice of pair (p_1, t_b) . This process is repeated for a representative range of p_1 and t_b . We use a least-squares best-fit algorithm to obtain the coefficients of the divergent, subdivergent, and UV cutoff-independent pieces as functions of t_b and p_1 .

3 Results

3.1 Confinement/deconfinement transition

We first describe the behavior of the extremal surfaces in the bulk.³ The possibility that extremal surfaces will bend toward the singularity and reach it at some nonzero value of the boundary time t_b may appear to be a concern, as this would make it impossible to evaluate the entanglement entropy at any earlier time. We find that this does not occur. The bulk time t increases along the extremal surface, reaching a maximum t_* at the midpoint $x = 0$. For t_b of order one, the increase is small (of order a few percent), but closer to the singularity it becomes larger. For example, for $p_1 = -0.25$ and $t_b = 0.4$, t_* is 20% larger than t_b .

Next we consider the radial extent of the extremal surface. For a static strip in pure AdS₆, the extremal surface reaches a maximum value of z given by [27]

$$z_* = \frac{4\Gamma(9/8)}{\sqrt{\pi}\Gamma(5/8)}\mathcal{L} \approx 1.48\mathcal{L} \quad (3.1)$$

where \mathcal{L} is the width of the strip. We find that this formula works remarkably well for the Kasner-AdS soliton with \mathcal{L} interpreted as the proper width of the entangling region, until z_* gets close to one. The fact that the cap in the radial direction due to the soliton does not affect the surface much when $z_* < 1$ can be understood from the fact that we work in six dimensions, so the effect of the cap comes in at $O(z^5)$ in (2.5). It is more surprising that the time dependence does not seem to affect the radial extent of the extremal surface (at least in the coordinates used in (2.5)). Eq. (3.1) holds even when the extremal surface does not stay near a constant t surface in the bulk.

When z_* does approach one, there is a qualitative change in the extremal surface. Rather than one surface connecting the two ends of the strip, the extremal surface splits into two pieces, with each one wrapping the cap at $z = 1$ (see Fig. 1). The topology of the extremal surface in the x, z, θ directions changes from $\mathbb{R} \times S^1$ to two copies of \mathbb{R}^2 . Once the extremal surface splits, the entanglement entropy becomes independent of the width \mathcal{L} .

This transition is the holographic description of a confinement/deconfinement phase transition [3, 4]. Entanglement entropy of a confining gauge theory measures the effective degrees of freedom between the entangling region and its complement at the energy scale $E \sim \frac{1}{\mathcal{L}}$. The corresponding modes of the gauge theory are in the deconfined phase when E is large and the entanglement entropy is a function of \mathcal{L} . As \mathcal{L} grows, one probes progressively lower energy modes. Eventually

³The specific calculations described in this section were done with $x_0 = 0.12$. This is a convenient value since it is large enough that the extremal surfaces do not stay just in the asymptotic AdS region, and small enough that the extremal surfaces stay connected for a range of t_b . It is worth noting that while $x_0 = 0.12$ is a convenient choice for the numerical analysis, the qualitative behavior is independent of this choice.

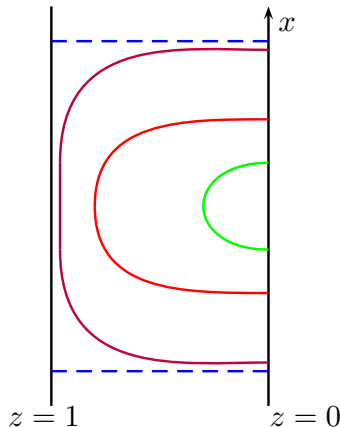


Figure 1: For small proper width \mathcal{L} in the Kasner-AdS soliton background, the extremal surfaces remain close to the boundary and resemble surfaces in pure AdS. The area of the surface depends on \mathcal{L} , so the entanglement entropy is a function of \mathcal{L} and the modes which contribute are deconfined. As the length of the entangling region becomes larger, extremal surfaces extend further into the bulk. The soliton cap begins to affect their geometry, and they start leveling out. For some critical length, the surface splits into two separate surfaces (displayed above in dashed blue). At this point, the area of the extremal surface is independent of \mathcal{L} , effectively signaling that $1/\mathcal{L}$ is below the mass gap of the confined gauge theory.

one hits the mass gap for the confining theory and there are no modes of lower energy. When this happens, the entanglement entropy becomes independent of \mathcal{L} .

The sign of p_1 clearly plays an important role in determining when this transition occurs. When $p_1 < 0$, the proper length \mathcal{L} grows as one approaches the singularity and the confinement/deconfinement transition takes place at early time. When $p_1 > 0$, \mathcal{L} grows as one moves away from the singularity, so the confinement/deconfinement transition occurs at late time (see Fig. 2).

3.2 Entanglement entropy

We now proceed to present the behavior of the area of the extremal surface as a function of t_b and p_1 . As noted above, this is divergent, so we introduce a small cutoff at $Z = \epsilon$ and expand $A(Z = \epsilon)$. It is convenient to factor out the trivial integral over y_1, y_2, θ and write:

$$\frac{A(\epsilon)}{L_1 L_2 \frac{4\pi}{5}} = \frac{c_3}{\epsilon^3} + \frac{c_1}{\epsilon} + c_0 + \dots \quad (3.2)$$

As expected, the subdivergent piece $1/\epsilon^2$ vanishes, and the leading coefficient is proportional to the area of the entangling region:

$$c_3 = \frac{1}{3} \frac{A_{\text{bdy}}}{L_1 L_2 \frac{4\pi}{5}} = \frac{2}{3} t_b^{p_2+p_3} = \frac{2}{3} t_b^{1-p_1} \quad (3.3)$$

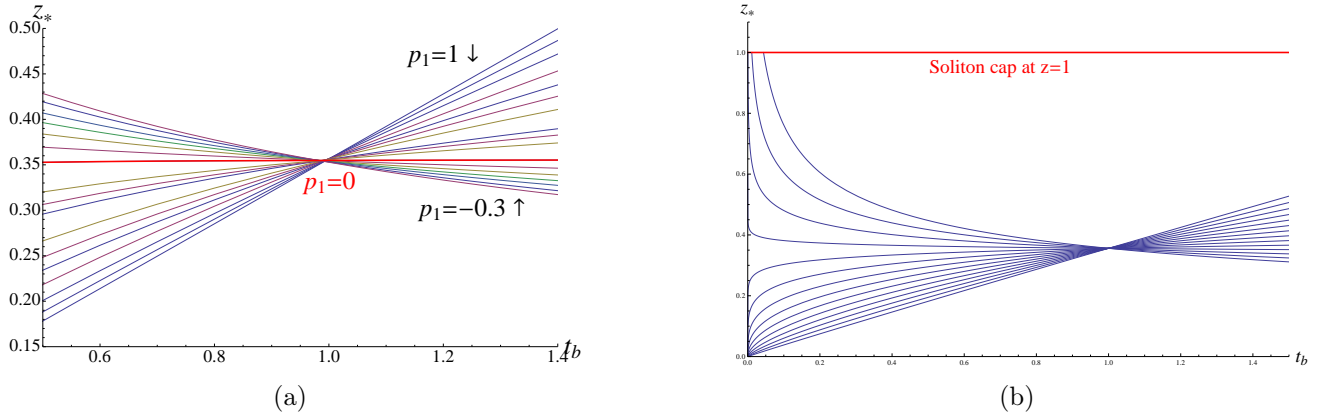


Figure 2: (a): The maximum value of z as a function of t_b , the boundary time. Each line corresponds to a different value of $p_1 \in [-0.3, 1]$: surfaces with positive p_1 shrink towards the boundary as $t_b \rightarrow 0$ while surfaces with $p_1 < 0$ approach the cap. Surfaces with $p_1 = 0$ maintain constant z_* . (b): A plot of $z_*(t_b) = 1.48\mathcal{L}$ for small t_b and $p_1 \in [-\frac{1}{3}, 1]$. This describes the radial extent of minimal surfaces until $z_* \approx 1$ when the surface splits into two, signaling a confinement/deconfinement transition.

where the factor of 2 is due to the fact that the y_i and θ are maximally extended, so $\partial\mathcal{R}$ consists of two identical disconnected pieces. The last equality comes from the Kasner conditions (2.2). The factor of $1/3$ in the first equality can be understood geometrically: the bulk is asymptotically locally AdS_6 , so near $Z = 0$, the area functional is approximately:

$$A_{\text{AdS}} = \int \frac{A_{\text{bdy}}}{Z^4} dZ \quad (3.4)$$

The Z^4 factor results in a $1/3$ contribution to the integral. This result moreover agrees with [5], where the computation is done for the pure soliton for an entangling region identical to $\mathcal{R}(t_b, x_0)$.

We next turn to the subleading divergence. We find $c_1(t_b)$ is a simple power law:

$$\begin{aligned} c_1(t_b) &= \gamma(p_1) t_b^{\beta(p_1)} \\ \gamma(p_1) &= a + bp_1 + cp_1^2 \\ \beta(p_1) &= -1 - p_1 \end{aligned} \quad (3.5)$$

where a , b , and c are numerical constants.

Considerations of covariance and dimensional analysis lead us to conclude that the c_1 coefficient is an integral of a dimension two geometric quantity. This can be the scalar curvature of the background spacetime, the induced metric on the boundary of the entangling region, or a scalar constructed from the square of the extrinsic curvature, $K_{\mu\nu}{}^\rho$. Both scalar curvatures vanish in our case, so the two possible contributions are:

$$A_{\text{bdy}} \left(\gamma_1 K_{\mu}{}^{\rho} K_{\nu}{}^{\rho} + \gamma_2 K_{\mu\nu}{}^{\rho} K^{\mu\nu}{}_{\rho} \right) = -\frac{A_{\text{bdy}}}{t_b^2} \left[\gamma_1 (1 - p_1)^2 + \gamma_2 (1 - p_1^2) \right] \quad (3.6)$$

for some constants γ_1 and γ_2 determined by the field theory. We therefore expect:

$$c_1 = 2t_b^{-1-p_1} \left[-(\gamma_1 + \gamma_2) + 2p_1\gamma_1 + (\gamma_2 - \gamma_1)p_1^2 \right] \quad (3.7)$$

The power of t_b in the time dependence of this expected behavior matches our results, $\beta(p_1) = -1 - p_1$. We may calculate γ_1 and γ_2 by setting the quadratic prefactors in (3.5) and (3.7) equal:

$$\frac{1}{2}(a + bp_1 + cp_1^2) = -(\gamma_1 + \gamma_2) + 2p_1\gamma_1 + (\gamma_2 - \gamma_1)p_1^2 \quad (3.8)$$

In other words:

$$\begin{aligned} \gamma_1 &= \frac{b}{4} \\ \gamma_2 &= -\frac{1}{2}\left(a + \frac{b}{2}\right) = \frac{1}{2}\left(c + \frac{b}{2}\right) \end{aligned} \quad (3.9)$$

This is an overdetermined system and has no solution unless $a = -(b + c)$. We find that our coefficients indeed satisfy this relation and furthermore determine $\gamma_1 \approx -0.1032$ and $\gamma_2 \approx 0.0238$. To the best of our numerical accuracy, these constants have a simple ratio $\frac{\gamma_1}{\gamma_2} = -\frac{13}{3}$. This is sufficient to determine the extrinsic curvature contributions to the $1/\epsilon$ divergence in general for a six dimensional bulk.

We now discuss the UV finite part of the entanglement entropy, $c_0(t_b)$. This is always negative, but has several qualitatively different behaviors depending on the value of p_1 . Recall that for a static strip in pure AdS₆, c_0 behaves as [24]:

$$c_{0, \text{ static}} \propto \frac{A_{\text{bdy}}}{x_0^3} \quad (3.10)$$

A naïve generalization of this for a time-dependent metric would be:

$$c_0 \propto \frac{A_{\text{bdy}}}{\mathcal{L}^3} \quad (3.11)$$

where, as before, \mathcal{L} is the proper width of the entangling region. We expect to find agreement with (3.11) for the Milne soliton ($p_1 = 1$) since this is static by the coordinate transformation (2.10). Indeed, we find that for p_1 between 1 and approximately 1/2, $c_0(t_b)$ is well fit by a simple power law

$$c_0 \propto t_b^{1-4p_1} = \frac{t_b^{1-p_1}}{t_b^{3p_1}} \propto \frac{A_{\text{bdy}}}{\mathcal{L}^3} \quad (3.12)$$

The agreement with this power law is illustrated in Fig. 3. We can attribute this agreement to the fact that for $1/2 < p_1 \leq 1$, the time dependence in the x direction dominates over the time dependence in the y_i directions.

If c_0 obeyed (3.12) for all p_1 , there would be an abrupt change in the behavior of c_0 at the critical value $p_1^{(c)} = 1/4$: surfaces with $p_1 > p_1^{(c)}$ would have c_0 diverging at early t_b and going to zero at late t_b , while surfaces with $p_1 < p_1^{(c)}$ would have c_0 vanishing at earlier times and diverging at late times. This is not what we find. Instead, for $p_1 < 0.5$, $c_0(t_b)$ is no longer fit by a simple power law. Fig. 4 shows the behavior of c_0 for small, positive p_1 . For $1/4 < p_1 < 1/2$, c_0 is less steep at early times than the static case would predict, while still diverging. For $0 < p_1 < 1/4$, $|c_0(t_b)|$ decreases as one moves toward the singularity as suggested by (3.12), but eventually turns around and starts to increase. We believe that it will eventually diverge as $t_b \rightarrow 0$, although it

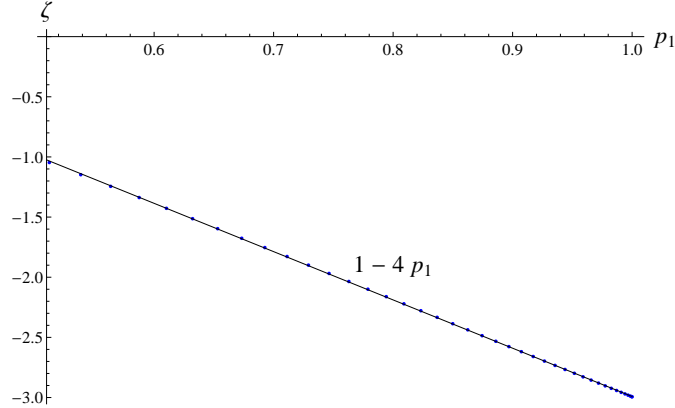


Figure 3: A plot of $\zeta(p_1)$, where $c_0(t) \propto t_b^{\zeta(p_1)}$, for $\frac{1}{2} < p_1 < 1$. The best-fit line is $\zeta(p_1) = 1 - 4p_1$.

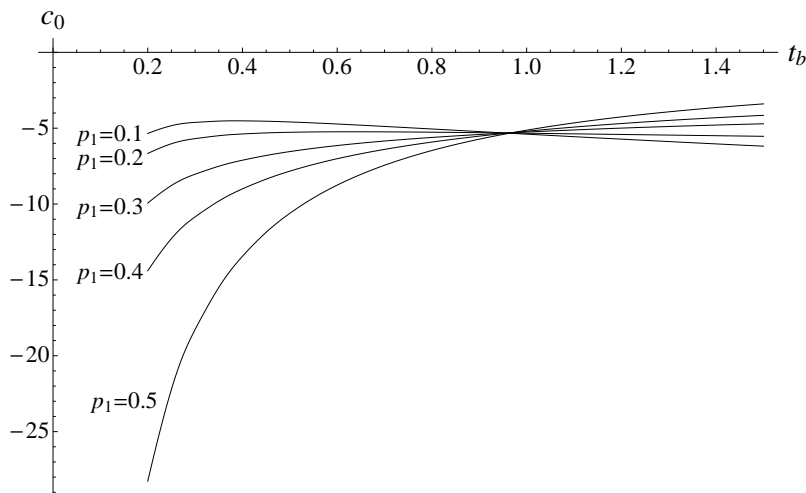


Figure 4: c_0 as a function of time for $0 < p_1 < 1/2$. As p_1 decreases, the c_0 curves level out, while still apparently diverging at early times, in contrast with the static prediction, which would imply that they go to zero for $p_1 < 1/4$.

is hard to numerically find the extremal surfaces very close to the singularity (and one cannot trust the classical bulk solution very close to the singularity anyway). For all of these cases, the width of the entangling region decreases at early times and the extremal surfaces stay close to the boundary. The fact that $|c_0(t_b)|$ diverges at early time likely stems from the fact that it is measuring entanglement of modes with shorter and shorter wavelength.

It is clear from Fig. 4 that all the curves cross at $t_b \approx 0.95$. In other words, $c_0(0.95)$ is essentially independent of p_1 . This is a result of the fact that for $t \approx 1$, the Kasner metric is independent of p_1 , and hence the same is true for the Kasner-AdS soliton. Since the extremal surfaces are staying close to a constant t surface when $t \approx 1$, their area is essentially independent of p_1 .

Finally, for $p_1 < 0$, $|c_0(t_b)|$ monotonically decreases at early times as illustrated in Fig. 5. In this case, the proper width of the entangling region grows and the extremal surface probes progressively deeper into the bulk. This is expected to continue until the confinement/deconfinement transition

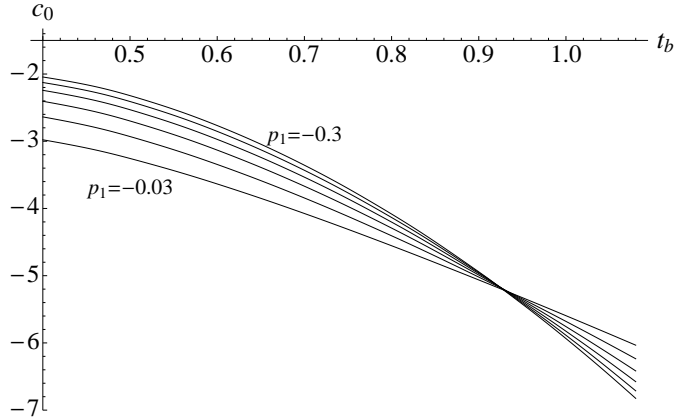


Figure 5: c_0 as a function of time for $-0.3 < p_1 < 0$. The curves correspond to $p_1 = -0.03, -0.11, -0.17, -0.22, -0.26,$ and -0.30 .

occurs, when the extremal surface hits the cap of the soliton and splits into two disconnected surfaces.

To summarize, we have computed the entanglement entropy of a confining gauge theory in a background spacetime which is a product of Kasner and a circle. In addition to the leading divergence which is proportional to the area, we found a subleading divergence proportional to the square of the extrinsic curvature of the entangling region. Near the singularity, we find that the behavior of the UV finite part of the entropy, c_0 , can differ significantly from the naïve extrapolation of the static result: the behavior of the width of our entangling strip is more important than the behavior of the area of its boundary. If the width goes to zero at early time, then c_0 diverges, while if it grows, then $|c_0(t_b)|$ decreases near the singularity and eventually reaches a confinement/deconfinement transition. This shows that the approach to the singularity can be used to determine the energy scale at which a confinement/deconfinement phase transition occurs in a gapped field theory.

In cosmology, one often considers states with nonzero temperature, and a confinement/ deconfinement transition occurs at a time when the temperature reaches a critical value. In contrast, we are not working with a state with nonzero temperature. Our state is given implicitly by our choice of bulk solution (since different states in the dual field theory correspond to different bulk geometries). However, one cannot describe this state as a vacuum state since the time dependence of the background causes particle creation. A vacuum state at one moment of time will not remain the vacuum at later time. This particle creation is contributing to $c_0(t_b)$.

It would be interesting to compare our calculation of the entanglement entropy, which is appropriate for a strongly coupled confining theory, with the entanglement entropy of a free field in Kasner (see, e.g., [28]).

Acknowledgements

We would like to acknowledge helpful discussions with Sebastian Fischetti, William Kelly, Rob Myers, Jorge Santos, Omid Saremi, and Benson Way. This work is supported in part by the National Science Foundation Graduate Research Fellowship under Grant No. DGE-1144085, and by NSF Grant No. PHY12-05500.

References

- [1] A. Kitaev and J. Preskill, “Topological entanglement entropy,” *Phys. Rev. Lett.* **96**, 110404 (2006) [hep-th/0510092].
- [2] M. Levin and X. G. Wen “Detecting topological order in a ground state wave function” *Phys. Rev. Lett* **96**, 110405 (2006) arXiv:0510613 [cond-mat.str-el]
- [3] T. Nishioka and T. Takayanagi, “AdS Bubbles, Entropy and Closed String Tachyons,” *JHEP* **0701**, 090 (2007) [hep-th/0611035].
- [4] I. R. Klebanov, D. Kutasov and A. Murugan, “Entanglement as a probe of confinement,” *Nucl. Phys. B* **796** (2008) 274 [arXiv:0709.2140 [hep-th]].
- [5] M. Ishihara, F. -L. Lin and B. Ning, “Refined Holographic Entanglement Entropy for the AdS Solitons and AdS black Holes,” arXiv:1203.6153 [hep-th].
- [6] B. Craps, S. Sethi and E. P. Verlinde, “A Matrix big bang,” *JHEP* **0510**, 005 (2005) [hep-th/0506180].
- [7] T. Hertog and G. T. Horowitz, “Holographic description of AdS cosmologies,” *JHEP* **0504**, 005 (2005) [hep-th/0503071].
- [8] N. Turok, B. Craps and T. Hertog, “From big crunch to big bang with AdS/CFT,” arXiv:0711.1824 [hep-th]; “On the Quantum Resolution of Cosmological Singularities using AdS/CFT,” *Phys. Rev. D* **86**, 043513 (2012) [arXiv:0712.4180 [hep-th]].
- [9] C. P. Burgess and L. McAllister, “Challenges for String Cosmology,” *Class. Quant. Grav.* **28**, 204002 (2011) [arXiv:1108.2660 [hep-th]].
- [10] H. Satz, “The Thermodynamics of Quarks and Gluons,” *Lect. Notes Phys.* **785**, 1 (2010) [arXiv:0803.1611 [hep-ph]].
- [11] S. Ryu and T. Takayanagi, “Holographic derivation of entanglement entropy from AdS/CFT,” *Phys. Rev. Lett.* **96** (2006) 181602 [hep-th/0603001].

- [12] V. E. Hubeny, M. Rangamani and T. Takayanagi, “A Covariant holographic entanglement entropy proposal,” JHEP **0707**, 062 (2007) [arXiv:0705.0016 [hep-th]].
- [13] J. Abajo-Arastia, J. Aparicio and E. Lopez, “Holographic Evolution of Entanglement Entropy,” JHEP **1011**, 149 (2010) [arXiv:1006.4090 [hep-th]].
- [14] J. Aparicio and E. Lopez, “Evolution of Two-Point Functions from Holography,” JHEP **1112**, 082 (2011) [arXiv:1109.3571 [hep-th]].
- [15] T. Albash and C. V. Johnson, “Evolution of Holographic Entanglement Entropy after Thermal and Electromagnetic Quenches,” New J. Phys. **13**, 045017 (2011) [arXiv:1008.3027 [hep-th]].
- [16] V. Balasubramanian, A. Bernamonti, J. de Boer, N. Copland, B. Craps, E. Keski-Vakkuri, B. Muller and A. Schafer *et al.*, “Thermalization of Strongly Coupled Field Theories,” Phys. Rev. Lett. **106**, 191601 (2011) [arXiv:1012.4753 [hep-th]]; “Holographic Thermalization,” Phys. Rev. D **84**, 026010 (2011) [arXiv:1103.2683 [hep-th]].
- [17] C. T. Asplund and S. G. Avery, “Evolution of Entanglement Entropy in the D1-D5 Brane System,” Phys. Rev. D **84**, 124053 (2011) [arXiv:1108.2510 [hep-th]].
- [18] P. Basu and S. R. Das, “Quantum Quench across a Holographic Critical Point,” JHEP **1201**, 103 (2012) [arXiv:1109.3909 [hep-th]].
- [19] P. Basu, D. Das, S. R. Das and T. Nishioka, “Quantum Quench Across a Zero Temperature Holographic Superfluid Transition,” arXiv:1211.7076 [hep-th].
- [20] J. Maldacena and G. L. Pimentel, “Entanglement entropy in de Sitter space,” JHEP **1302**, 038 (2013) [arXiv:1210.7244 [hep-th]].
- [21] A. Buchel, L. Lehner, R. C. Myers and A. van Niekerk, “Quantum quenches of holographic plasmas,” arXiv:1302.2924 [hep-th].
- [22] M. Nozaki, T. Numasawa and T. Takayanagi, “Holographic Local Quenches and Entanglement Density,” arXiv:1302.5703 [hep-th].
- [23] T. Hartman and J. Maldacena, “Time Evolution of Entanglement Entropy from Black Hole Interiors,” arXiv:1303.1080 [hep-th].
- [24] T. Nishioka, S. Ryu and T. Takayanagi, “Holographic Entanglement Entropy: An Overview,” J. Phys. A **42**, 504008 (2009) [arXiv:0905.0932 [hep-th]].
- [25] E. Witten, “Anti-de Sitter space, thermal phase transition, and confinement in gauge theories,” Adv. Theor. Math. Phys. **2**, 505 (1998) [hep-th/9803131].
- [26] G. T. Horowitz and R. C. Myers, “The AdS / CFT correspondence and a new positive energy conjecture for general relativity,” Phys. Rev. D **59**, 026005 (1998) [hep-th/9808079].

- [27] V. E. Hubeny, “Extremal surfaces as bulk probes in AdS/CFT,” JHEP **1207**, 093 (2012) [arXiv:1203.1044 [hep-th]].
- [28] H. Casini and M. Huerta, “Entanglement entropy in free quantum field theory,” J. Phys. A **42**, 504007 (2009) [arXiv:0905.2562 [hep-th]].